



## Evaluating CERES angular distribution models for snow using surface reflectance observations from the East Antarctic Plateau

Stephen R. Hudson,<sup>1</sup> Seiji Kato,<sup>2</sup> and Stephen G. Warren<sup>3</sup>

Received 10 June 2009; revised 14 September 2009; accepted 17 September 2009; published 3 February 2010.

[1] Clouds and the Earth's radiant energy system (CERES) is a satellite-based remote sensing system designed to monitor the Earth's radiation budget. In this paper we examine uncertainties in the angular distribution models (ADMs) used by CERES over permanently snow covered surfaces with clear skies. These ADMs are a key part of the CERES data processing algorithms, used to convert the observed upwelling radiance to an estimate of the upwelling hemispheric flux. We model top-of-atmosphere anisotropic reflectance factors using an atmospheric radiative transfer model with a lower boundary condition based on extensive reflectance observations made at Dome C, Antarctica. The model results and subsequent analysis show that the CERES operational clear-sky permanent-snow ADMs are appropriate for use over Dome C, with differences of less than 5% between the model results and the ADMs at most geometries used by CERES operationally. We show that the uncertainty introduced into the flux estimates through the use of the modeled radiances used in the ADM development is small when the fluxes are averaged over time and space. Finally, we show that variations in the angular distribution of radiance at the top of the atmosphere due to atmospheric variability over permanently snow covered regions are in most cases unlikely to mask the real variations in flux caused by these atmospheric variations.

**Citation:** Hudson, S. R., S. Kato, and S. G. Warren (2010), Evaluating CERES angular distribution models for snow using surface reflectance observations from the East Antarctic Plateau, *J. Geophys. Res.*, 115, D03101, doi:10.1029/2009JD012624.

### 1. Introduction

[2] Clouds and the Earth's radiant energy system (CERES) is a suite of satellite-based instruments designed to monitor the Earth's radiation budget [Wielicki *et al.*, 1996]. The successor to the Earth Radiation Budget Experiment (ERBE), CERES is designed to double the accuracy of the ERBE observations through the use of improved instruments and analysis techniques. Data products produced by the CERES team include the observed broadband solar, window longwave, and broadband longwave radiances, along with many derived products, including fluxes in the three channels at the top of the atmosphere (TOA) and the surface.

[3] CERES consists of five instruments on three satellites, and a sixth instrument to be placed on the satellite that will be launched for the NPOESS (National Polar-Orbiting Operational Environmental Satellite System) preparatory project (NPP). Two of the satellites, Aqua and Terra, each have two instruments on board. These two are polar-orbiting satellites, so they frequently observe the East Antarctic Plateau. In

addition to the broadband radiance observations from the CERES instruments, the CERES algorithms make use of spectral observations from the Moderate Resolution Imaging Spectroradiometer (MODIS), which also flies on Aqua and Terra, to determine the scene type over CERES footprints, such as cloud fraction, optical thickness, and droplet size.

[4] One of the primary goals of the CERES experiment is to determine the TOA radiation budget of all regions of the planet. To do this the CERES-observed instantaneous radiances must be converted to estimates of the instantaneous upwelling flux. Doing this conversion requires an angular distribution model (ADM) that predicts the upwelling flux, given the radiance at any one viewing angle. These ADMs were developed by combining all radiance observations made over a given surface type, with a given cloud fraction, and calculating the average radiance in each viewing angle bin as a function of solar zenith angle [Loeb *et al.*, 2005].

[5] In this paper we use a parameterization of surface reflection developed for the East Antarctic Plateau along with an atmospheric radiative transfer model to assess the uncertainty associated with the shortwave ADMs used by CERES for clear-sky, permanently snow covered scenes. These ADMs are described in detail by Kato and Loeb [2005]. We also examine how the atmosphere modifies the angular distribution of reflected radiance between the surface and TOA, and how variations in atmospheric properties may affect the TOA radiance field, introducing errors into the estimated fluxes.

<sup>1</sup>Norwegian Polar Institute, Tromsø, Norway.

<sup>2</sup>Climate Science Branch, NASA Langley Research Center, Hampton, Virginia, USA.

<sup>3</sup>Department of Atmospheric Sciences, University of Washington, Seattle, Washington, USA.

[6] The main quantity considered in this paper is the anisotropic reflectance factor, defined as

$$R(\theta_o, \theta_v, \phi) = \frac{\pi I_r(\theta_o, \theta_v, \phi)}{\int_0^{2\pi} \int_0^{\pi/2} I_r(\theta_o, \theta_v, \phi) \cos \theta_v \sin \theta_v d\theta_v d\phi}, \quad (1)$$

where  $I_r$  is the radiance reflected into the viewing zenith angle  $\theta_v$  and relative azimuth angle  $\phi$ , with solar zenith angle  $\theta_o$ . The denominator in equation (1) is the reflected flux. CERES is a broadband instrument, so the quantities are integrated over the solar spectrum. The CERES ADMs consist of estimates of  $R(\theta_o, \theta_v, \phi)$  made by averaging  $I_r$  over bins in  $\theta_o$ ,  $\theta_v$ , and  $\phi$ . Using these ADMs, a reflected flux can be estimated from a CERES radiance observation using

$$F_r = \frac{\pi I_r(\theta_o, \theta_v, \phi)}{R(\theta_o, \theta_v, \phi)}. \quad (2)$$

The uncertainty in the ADMs is important since the relative error of the derived flux ( $F_r$ ) is equal to the relative difference between the actual value of  $R$  and the ADM estimate of  $R$ .

## 2. Model

[7] The model results presented in this paper come from SBDART, a package for modeling radiative transfer in the atmosphere [Ricchiuzzi *et al.*, 1998]. SBDART is built around the plane-parallel radiative transfer model DISORT [Stamnes *et al.*, 1988] and uses the band models developed for LOWTRAN 7 for atmospheric gaseous absorption.

[8] The model was modified to use the parameterizations for the bidirectional reflectance of snow from the work of Hudson *et al.* [2006] to determine the bidirectional reflectance factor (BRF; equal to  $R$  times the albedo) of the surface. These parameterizations were developed from extensive radiance measurements made from 32 m above the surface at Dome C Station, Antarctica (75°S, 123°E, 3200 m). Because these parameterizations do not cover all wavelengths or incidence angles, certain assumptions and extensions had to be made since CERES observes the full solar spectrum and the model must be able to calculate the BRF for all incidence angles to handle diffuse incidence. Three assumptions regarding the variation of  $R$  with incidence angle were made for all wavelengths:  $R$  for incident zenith angles greater than 86.6° is equal to the parameterized  $R$  for 86.6°;  $R$  for an incidence angle of 0° is equal to 1 at all viewing angles (isotropic reflectance);  $R$  for incidence angles between 0° and 51.6° is the linear interpolation, in cosine of the incidence angle, between the isotropic reflection at 0° and the parameterized  $R$  at 51.6°. At visible wavelengths  $R$  is not far from isotropic even at  $\theta_o = 51.6^\circ$ , while at longer wavelengths there is very little diffuse incidence, so little error should result from the interpolation. All wavelengths between 0.2 and 0.8  $\mu\text{m}$  use  $R(\lambda = 0.8 \mu\text{m})$  to avoid the effect of diffuse radiation in the observations, as discussed in section 5.3 of Hudson *et al.* [2006].

[9] Hudson *et al.* [2006] did not provide parameterizations valid for  $R$  at all wavelengths and incidence angles; no parameterization was provided for wavelengths with albedo less than 0.15 or between 0.27 and 0.47 for any incidence angles, nor for wavelengths with albedo between 0.15 and

0.27 for incidence angles greater than 75°. For wavelengths with albedo between 0.27 and 0.47,  $R$  was determined with a new parameterization developed with the same method used by Hudson *et al.* [2006], but with their data from wavelengths 1.39 to 1.51  $\mu\text{m}$ . Interpolation in a lookup table of  $R(\theta_o = 82.6^\circ)$  as a function of albedo was used to find  $R$  for all incidence angles greater than 75° at wavelengths with albedo ( $\alpha$ ) between 0.15 and 0.27. For wavelengths with albedo less than 0.15,  $R$  was set to the parameterized values of  $R$  at albedo equal to 0.15 if the incidence angle was less than 75°, or to  $R(\alpha = 0.15, \theta_o = 82.6^\circ)$  if the incidence angle was greater than 75°.

[10] The parameterization requires knowledge of the surface albedo under diffuse illumination at all wavelengths beyond 0.95  $\mu\text{m}$ , but the albedo at Dome C was measured only at wavelengths out to 2.4  $\mu\text{m}$ . To estimate the albedo at other wavelengths, SBDART was used to model the spectral albedo of a snowpack consisting of a 0.25 mm layer of 40  $\mu\text{m}$  ice spheres above a semi-infinite layer of 90  $\mu\text{m}$  ice spheres (the sizes that resulted in a best fit to the observed albedo between 0.35 and 2.4  $\mu\text{m}$ , as described in section 4 of Hudson and Warren [2007]) at wavelengths from 0.2 to 10  $\mu\text{m}$  under a cloud that diffused the solar beam. These albedo values were used in the parameterization at wavelengths where the albedo was not observed.

[11] The assumptions listed above allow the parameterizations to be extended to provide  $R$  for all necessary wavelengths and incidence angles, but DISORT needs the BRF, not  $R$ ; the two differ by a factor of the surface albedo. In this case the surface albedo that is used should vary with incidence angle; this variation is especially important at near-infrared wavelengths. A table of albedo as a function of solar zenith angle ( $\theta_o = 0^\circ, 1^\circ, 2^\circ, \dots, 89^\circ$ ) and wavelength ( $\lambda = 0.2 \mu\text{m} \times 1.016^n, n = 0, 1, 2, \dots, 250$ ) was calculated with SBDART for the same snowpack as above, but with no atmosphere or cloud. Bilinear interpolation could then be used to determine the albedo at any wavelength between 0.2 and 10  $\mu\text{m}$  and any incidence angle. For the work in this paper, comparing values of  $R$ , for which the normalization by the reflected flux removes the effect of albedo bias, small errors in the magnitude of the spectral albedo are not very important, so long as the spectral shape is correct.

[12] At this point the model can estimate the BRF of the surface at all necessary wavelengths and incidence angles. The importance of many of the assumptions and estimates that went into the model is diminished by the fact that most of them primarily affect wavelengths longer than 1.4  $\mu\text{m}$ , where there is less incident solar radiation than at shorter wavelengths and where the snow has a low albedo (generally less than 0.3); about 85% of the incident solar flux and 94% to 98% of the reflected solar flux (depending on  $\theta_o$ ) at the TOA over Dome C is at wavelengths shorter than 1.4  $\mu\text{m}$ .

[13] Below 28 km, the temperature, pressure, and water vapor profiles used as input to SBDART were specified as the mean of 47 radiosoundings conducted at Dome C during January 2004 [Gettelman *et al.*, 2006]. Ozone concentration at all heights, and all quantities above 28 km, was taken from the summertime South Pole model atmosphere of Walden *et al.* [1998], who used ozonesonde data for ozone concentrations below 30 km, and various satellite data for all quantities above 30 km. No aerosols were used in the model; the mean observed clear-sky aerosol optical thickness at

Dome C during summer 2003–2004 was 0.02 at  $0.44 \mu\text{m}$  and 0.007 at  $0.87 \mu\text{m}$  [Six *et al.*, 2005]. Running the model with a layer of stratospheric aerosols with optical depth 0.02 at  $0.55 \mu\text{m}$  resulted in reflected flux calculations that differ from the standard model by 0.008% at  $\theta_o = 59^\circ$  and by 0.13% at  $\theta_o = 80^\circ$ , and resulted in reflected radiance calculations that differ from the standard model by less than 1% at  $\theta_o = 59^\circ$  and by less than 4.5% at  $\theta_o = 80^\circ$ , for  $\theta_v \leq 70^\circ$  (those most important to CERES). Radiance differences exceed 10% at large  $\theta_v$  in the forward-reflected direction.

[14] The model was run, with thermal emission turned off, over the wavelength range 0.2 to  $10 \mu\text{m}$ , with a wavelength interval of 0.02 times the current wavelength, resulting in 196 wavelengths, more closely spaced at shorter wavelengths, where the majority of the reflected energy is. DISORT was run with 24 streams and with its intensity correction algorithm turned on [Nakajima and Tanaka, 1988].

[15] The wavelength range 0.2 to  $10 \mu\text{m}$  was chosen to allow a comparison with the most widely used CERES shortwave products, which are based on the “unfiltered” radiances. The unfiltering process, described by Loeb *et al.* [2001], converts the measured radiance, which is affected by instrument filtering and thermal emission, to the total upwelling solar flux at all wavelengths. This is stated most clearly in the document describing the CERES SSF data product [Geier *et al.*, 2003], where the following is written on page 46: The unfiltered shortwave radiance “is an estimate of the solar radiance at all wavelengths reflected back into space and contains no thermal radiance. . . It is a spectrally integrated radiance that is intended to represent the radiance of reflected sunlight. In other words, the SW unfiltered radiance is the radiance we would observe if we had a spectrally flat channel that passed all the reflected sunlight and that removed any thermal emission from the Earth and the Earth’s atmosphere. Frequently, in informal discussion, we incorrectly refer to the SW unfiltered radiance as a broadband radiance covering the spectral interval from 0 to  $5 \mu\text{m}$ .”

[16] The model was run and output saved at the bin-center angles used in the CERES ADMs ( $\theta_o = 1^\circ, 3^\circ, 5^\circ, \dots, 89^\circ$ ;  $\theta_v = 2.5^\circ, 7.5^\circ, 12.5^\circ, \dots, 87.5^\circ$ ;  $\phi = 2.5^\circ, 7.5^\circ, 12.5^\circ, \dots, 177.5^\circ$ ), and the comparisons were then made directly.

### 3. Comparison with Angular Distribution Models

[17] The CERES team has developed two sets of ADMs for clear-sky observations over permanently snow covered surfaces: a bright permanent-snow ADM and a dark permanent-snow ADM [Kato and Loeb, 2005]. This brightness distinction was made to try to account for some of the snow-property changes that can affect the distribution of reflected radiance. MODIS  $0.645 \mu\text{m}$  reflectance observations near nadir during the 2-yr period of the ADM development data set were used to classify permanent-snow regions as bright or dark, on the basis of whether their monthly mean reflectance was greater or less than the mean reflectance from permanent snow (the evaluation was done as a function of solar zenith angle). Operationally, the CERES algorithms choose the bright or dark ADM on the basis of which one more closely matches the observation. The main difference between the two ADMs is their albedo.

[18] Each ADM provides the average TOA albedo as a function of solar zenith angle and the TOA  $R$  as a function of solar

zenith angle and viewing angles. They were developed using all clear-sky permanent-snow scenes observed by CERES, mostly the Greenland and Antarctic ice sheets. In this section they are compared with the TOA modeled  $R$  over Dome C. Since data from lower-elevation sites with more precipitable water and from locations and times with varying ozone concentrations were included in the ADM development, an exact match between the ADMs and the model should not be expected; nevertheless, the ADMs are used over Dome C, so these comparisons provide a useful estimate of their uncertainty. We expect that the agreement of  $R$  above different regions should be better than the agreement of radiances, and we show in section 5 that the variation in  $R$  caused by variations in precipitable water and ozone amount is small.

[19] Comparisons of  $R$  are shown in Figure 1. This figure shows the modeled values of  $R$  at two solar zenith angles and the difference between the values of  $R$  from the ADMs and the values of  $R$  from the model. Plots at other solar zenith angles show similar results. These plots show that, despite the different regions included in the CERES ADM development, the ADMs appear to be appropriate for use over Dome C.

[20] Most CERES observations that are used operationally are made with  $\theta_v < 70^\circ$ . At these angles, the differences between  $R$  from the CERES ADMs and  $R$  from the Dome-C model are mostly smaller than 5%. Larger errors, mostly negative, are found at large  $\theta_v$ , possibly because of including observations over moister atmospheres, since increased water vapor concentrations would reduce  $R$  more at large  $\theta_v$ , where the atmospheric path length is longer. These differences could also be due to other spatial or temporal variability, or to procedures used in the ADM development, in which viewing angles without data were filled with model results, which we investigate in section 4. Alternatively, they could represent error in the Dome-C model.

### 4. Estimate of the Flux Error Caused by the Modeled Radiance in Solar Avoidance Angles

[21] As described by Loeb *et al.* [2005] and Kato and Loeb [2005], CERES ADMs depend on scene type. Cloud fraction and cloud properties derived from MODIS are used to identify the scene type over a CERES footprint. At CERES viewing zenith angles greater than  $75^\circ$  around  $90^\circ$  relative azimuth angle, however, collocation of MODIS radiance with CERES footprints is not available. In addition, because CERES instruments avoid observing the direct solar beam, they do not scan beyond a viewing zenith angle of approximately  $60^\circ$  near  $0^\circ$  relative azimuth angle when the solar zenith angle is large. CERES radiances for use in building ADMs are, therefore, not available for these viewing angles. The Greenland Ice Sheet extends to nearly  $60^\circ\text{N}$  and, therefore, experiences a minimum solar zenith angle of about  $37^\circ$ ; the rest of Greenland and Antarctica, which include most of the permanent-snow scenes, lie farther poleward, so observations of permanent-snow scenes with  $\theta_o < 40^\circ$  are unusual. For  $\theta_o > 50^\circ$ , Figure 2 shows that the solid angle subtended by the area of missing observed radiances slightly increases with solar zenith angle. The fraction of the solid angle with no CERES radiances subtended in the upper hemisphere is, however, less than 10% for all solar zenith angles of interest over clear-sky permanent-snow scenes except for the bright snow surface scene with solar zenith angle  $89^\circ$ .

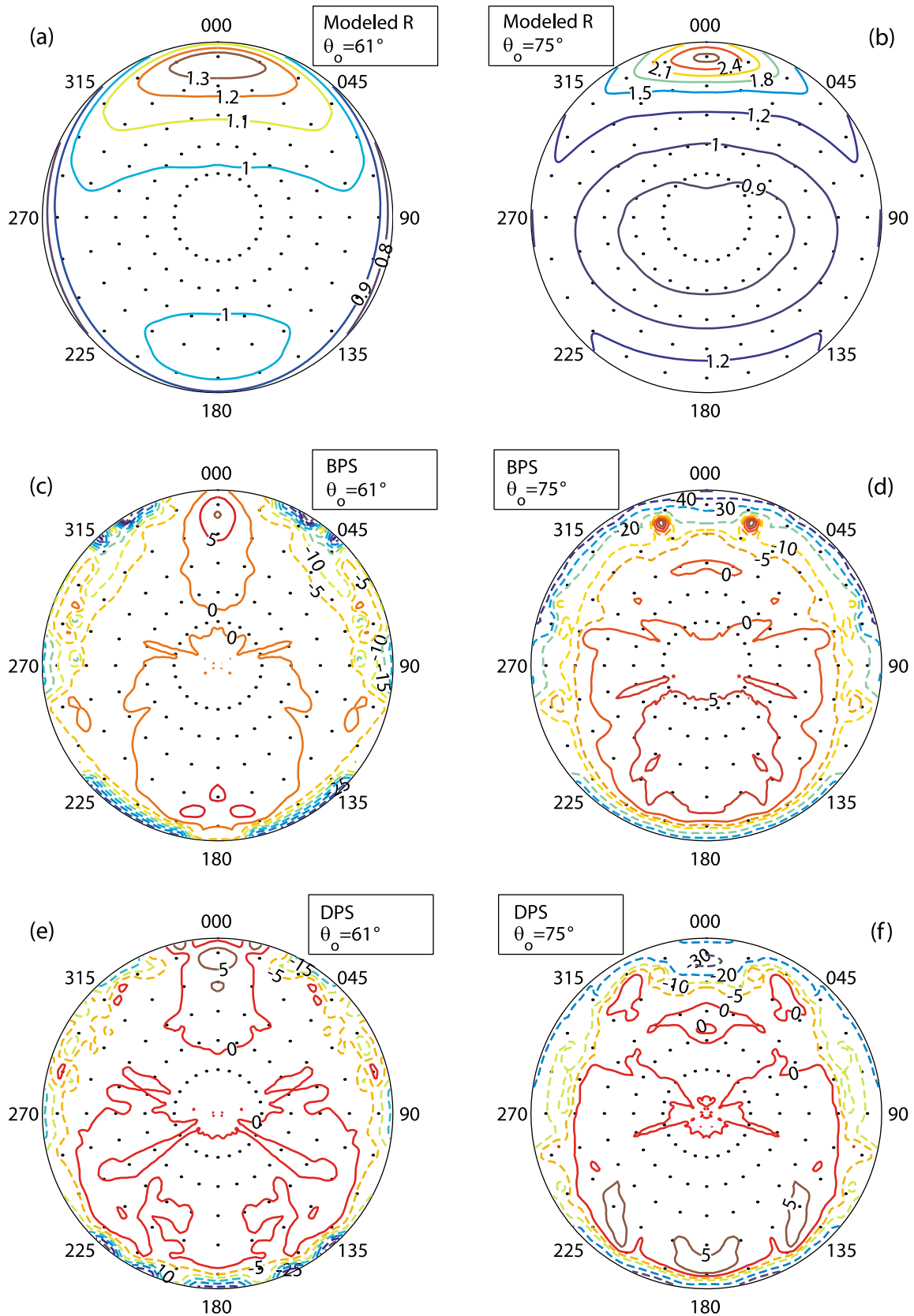


**Figure 1.** (a and b) The modeled TOA anisotropic reflectance factor ( $R$ ) values at solar zenith angles of  $61^\circ$  and  $75^\circ$ . (c–f) The relative difference (%) between  $R$  from the CERES bright (BPS) and dark (DPS) permanent-snow ADMs and the modeled  $R$  at the same two solar zenith angles. A negative difference indicates that CERES  $R$  is less than the modeled  $R$ . Dots are located every  $15^\circ$  in  $\phi$  and at  $\theta_v$  of  $22.5^\circ$ ,  $37.5^\circ$ ,  $52.5^\circ$ ,  $67.5^\circ$ , and  $82.5^\circ$ .

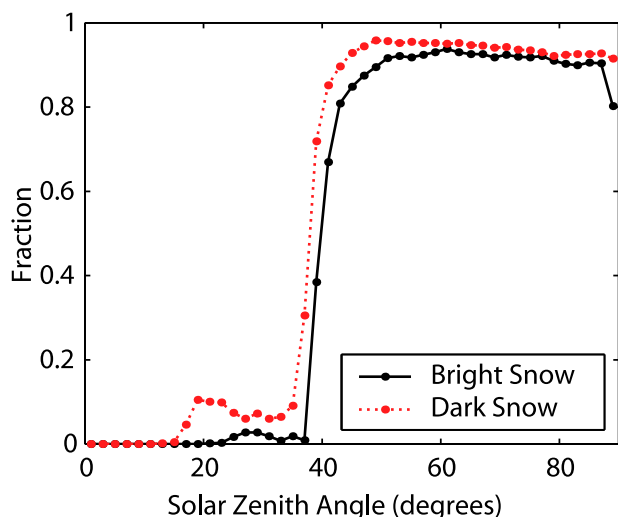


**Figure 2.** Fraction of the solid angle for which CERES radiances were available for building clear-sky bright-snow (solid line) and dark-snow (dotted line) ADMs as a function of solar zenith angle.

[22] Even though fluxes are not estimated from angles where CERES radiances are not used in ADMs, missing observed CERES radiances affect the flux in the following way. In the process of building CERES ADMs, the denominator of the right side of equation (1) is the mean flux (hereinafter ADM flux)  $\bar{F}$  computed by integrating the mean radiance  $\bar{I}$  over the hemisphere for a given scene type. The integration requires filling radiances at angles where CERES observations are not available. As described by *Loeb et al.* [2005] and *Kato and Loeb* [2005], modeled radiances were used at these angles. The error in the modeled radiance affects the anisotropic factor in equation (1), and subsequently affects the flux estimate from equation (2) where  $I$  is the instantaneous CERES observed radiance.

[23] Because of the small water vapor amount and small aerosol loadings over Antarctica, the largest uncertainty in modeling the clear-sky TOA radiance over permanent-snow surfaces is in the surface boundary condition, namely, the surface BRF. Note that the surface BRF parameterizations discussed in section 2 were not available when the CERES permanent-snow ADMs were developed. The snow surface BRF is difficult to model because of the existence of large-scale surface roughness caused by sastrugi [e.g., *Warren et al.*, 1998; *Leroux and Fily*, 1998]. Using a smooth surface packed with snow grains leads to a large error in modeling the snow surface BRF compared to observed surface BRF [e.g., *Jin and Simpson*, 1999]. Because the effect of large-scale surface roughness was neglected in modeling radiances over snow surfaces and because those radiances were used to fill radiances at angles with no CERES radiances for the CERES operational ADMs, the effect of modeling error in the flux estimate needs to be evaluated.

[24] The good agreement shown in section 3 between our model and the CERES ADMs indicates that the parameterized  $R$  used as the boundary condition in the model used in this paper represents the mean anisotropic factor of Antarctic permanent-snow surfaces. We can therefore use the anisotropic factors computed from surface BRF observations over Dome C to test the error caused by the modeled radiance used

in nonobserved angles for CERES operational clear-sky permanent-snow ADMs (hereinafter  $ADM_{ed3}$ ).

[25] To test the error, we built clear-sky permanent-snow ADMs by filling nonobserved angles with modeled radiances computed with the surface boundary condition constrained with observed surface BRF measurements over Dome C (hereinafter  $ADM_{fill}$ ). Following *Loeb et al.* [2005], we used only the shape of the modeled radiance as a function of angle. Figure 3 shows the relative difference of the ADM albedos,  $(\bar{\alpha}_{fill} - \bar{\alpha}_{ed3})/\bar{\alpha}_{ed3}$ , where  $\bar{\alpha}_{fill}$  and  $\bar{\alpha}_{ed3}$  are the ADM albedo from  $ADM_{fill}$  and from  $ADM_{ed3}$ , respectively. For  $\theta_o < 80^\circ$ , the error in the ADM albedo is less than 1% for both bright and dark snow. Larger values occur for  $\theta_o > 80^\circ$ .

[26] For climate studies, instantaneous fluxes are spatially and temporally averaged. Because the solar zenith angle and a CERES instrument viewing geometry over a  $1^\circ \times 1^\circ$  area change over the course of a month, and the sign of the error shown in Figure 3 changes with solar zenith angles between  $75^\circ$  and  $85^\circ$ , we expect the error in the monthly mean flux averaged over a  $1^\circ \times 1^\circ$  area to be smaller than the instantaneous flux error. To assess the error in the  $1^\circ \times 1^\circ$  gridded monthly mean clear-sky flux, we apply both  $ADM_{ed3}$  and  $ADM_{fill}$  to CERES data taken over Antarctica in January and March 2004. We then compare fluxes derived from the two sets of ADMs averaged over a month and over  $1^\circ \times 1^\circ$  areas. As shown in Figure 4a, the error in the gridded monthly mean flux in January is everywhere less than  $1.5 \text{ W m}^{-2}$ , which corresponds to approximately 0.5% of the mean reflected shortwave flux. The differences, averaged over the region  $70^\circ\text{S}$  to  $90^\circ\text{S}$  and over the Dome C region ( $74^\circ\text{S}$ – $76^\circ\text{S}$ ,  $120^\circ\text{E}$ – $125^\circ\text{E}$ ), are shown in Table 1.

[27] For a further comparison of the monthly mean flux error over  $1^\circ \times 1^\circ$  areas, we built another set of clear-sky permanent-snow ADMs using no CERES data, using only the reflectance model based on Dome-C surface measurements for all angles (hereinafter  $ADM_{replace}$ ). The comparison of the

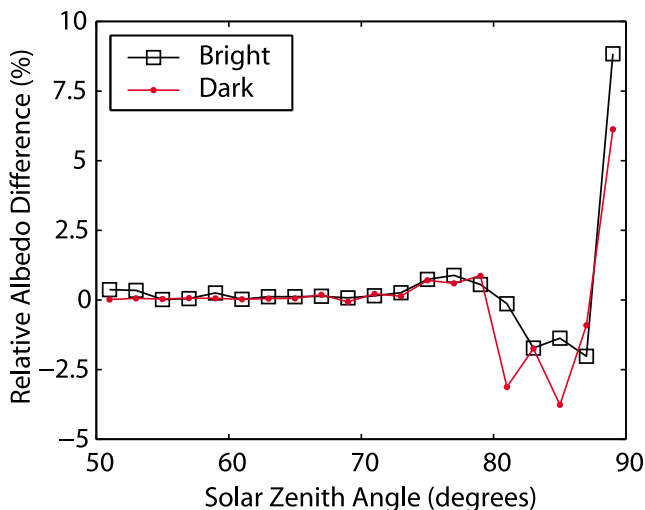


**Figure 3.** Relative difference in mean albedo (“ADM albedo”) between (1) CERES clear-sky permanent-snow ADMs ( $ADM_{ed3}$ ) and (2) ADMs with missing observed radiances filled by modeled radiances constrained with surface BRF measurements over Dome C ( $ADM_{fill}$ ), as a function of solar zenith angle. The relative difference is defined as  $(ADM_{fill} - ADM_{ed3})/ADM_{ed3}$ .

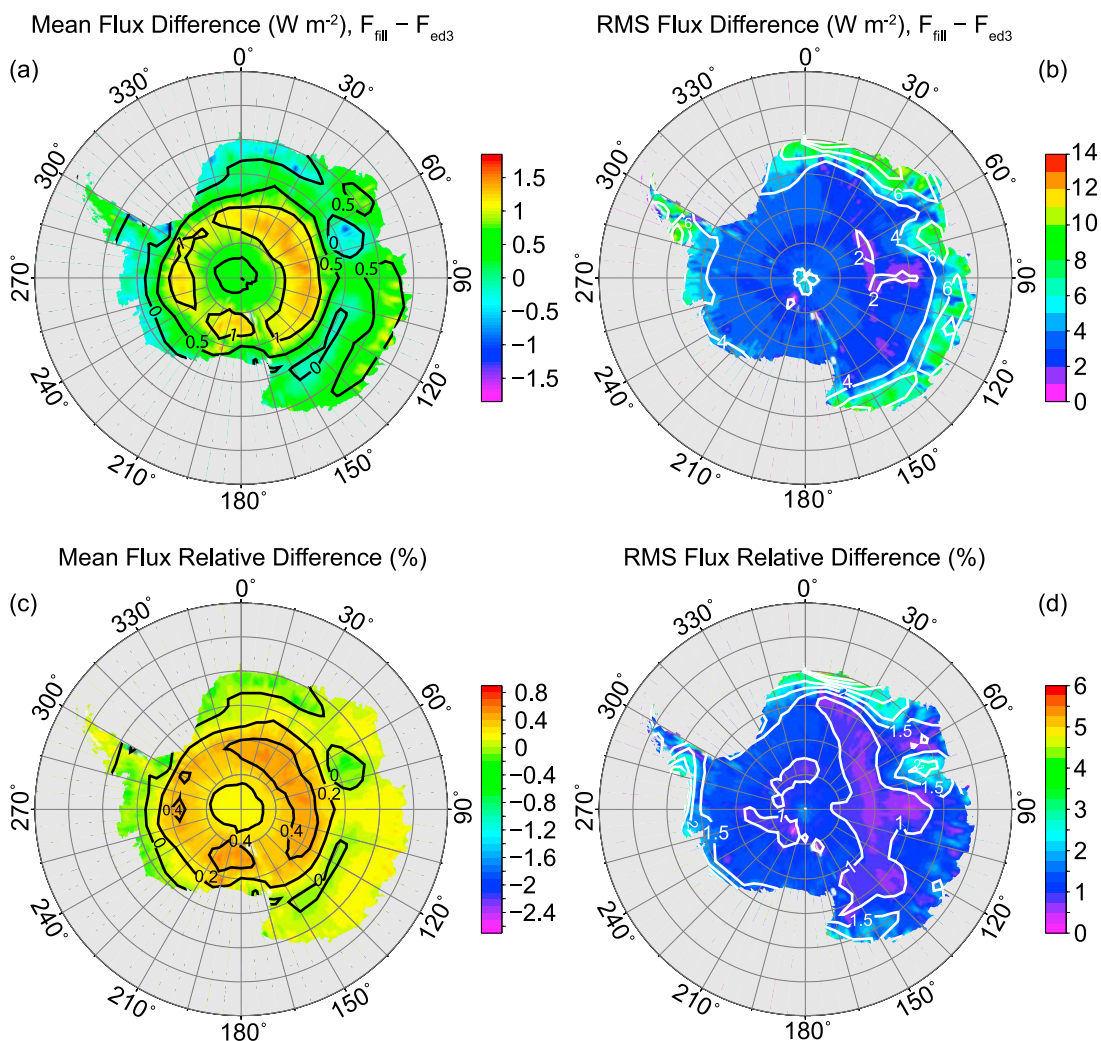


**Figure 4.** (a) Difference between monthly mean TOA reflected fluxes derived from  $ADM_{\text{fill}}$  and from  $ADM_{\text{ed3}}$  and (b) RMS difference of instantaneous fluxes derived from  $ADM_{\text{fill}}$  and from  $ADM_{\text{ed3}}$ , over Antarctica. (c and d) Values relative to those derived from  $ADM_{\text{ed3}}$ . January 2004 data were used for the plots. The contours were drawn from averages over bins of  $1^\circ$  in latitude and  $5^\circ$  in longitude; the full  $1^\circ \times 1^\circ$  resolution is shown in the color background.

monthly mean clear-sky flux derived from  $ADM_{\text{ed3}}$  and from  $ADM_{\text{replace}}$  provides a further consistency check of CERES radiances and modeled radiances based on the observed surface BRF over Dome C, evaluated by the difference in the monthly mean flux.

[28] Table 1 shows that the difference between monthly mean clear-sky fluxes derived from  $ADM_{\text{ed3}}$  and from  $ADM_{\text{replace}}$  is approximately twice the difference between the fluxes derived from the operational ADMs and from  $ADM_{\text{fill}}$ , but they still show reasonable agreement, with relative RMS differences less than 3%. The mean difference of the monthly mean clear-sky flux in January 2004 between  $70^\circ\text{S}$  and  $90^\circ\text{S}$  derived from  $ADM_{\text{fill}}$  and  $ADM_{\text{ed3}}$  is  $0.4 \text{ W m}^{-2}$  (0.2%) while the mean difference of the monthly mean flux derived from  $ADM_{\text{replace}}$  and  $ADM_{\text{ed3}}$  over the same region is  $1.4 \text{ W m}^{-2}$  (0.5%).

[29] These results are consistent with the result of *Kato and Loeb* [2005] who compared the clear-sky monthly mean flux derived from CERES operational ADMs and local ADMs over Antarctica and found that the mean difference was  $1.4 \text{ W m}^{-2}$ ,

where the flux derived from the local ADM was smaller. The less than 2% differences in the derived monthly mean fluxes are well within the uncertainty of the parameterization of  $R$ , discussed by *Hudson et al.* [2006]. In addition, the result is also consistent with measurements reported by *Hudson et al.* [2006] which showed that  $R$  at  $\lambda = 900 \text{ nm}$  observed at the South Pole and at Dome C are similar. All these results together imply that the effect on fluxes derived by CERES

**Table 1.** Mean and RMS Differences Between Regional, Monthly Mean Flux Calculations Using Different ADMs<sup>a</sup>

	January 2004		March 2004	
	$70^\circ\text{S}-90^\circ\text{S}$	Dome C	$70^\circ\text{S}-90^\circ\text{S}$	Dome C
$F_{\text{fill}} - F_{\text{ed3}}$				
Mean	0.4 (0.2%)	-0.1 (0.0%)	0.3 (0.2%)	0.9 (0.6%)
RMS	3.9 (1.5%)	2.5 (0.8%)	2.2 (1.6%)	2.6 (1.7%)
$F_{\text{replace}} - F_{\text{ed3}}$				
Mean	1.4 (0.5%)	1.6 (0.6%)	1.8 (1.4%)	3.2 (1.9%)
RMS	5.3 (2.0%)	6.8 (2.4%)	3.5 (2.6%)	4.1 (2.4%)

<sup>a</sup> Absolute differences are in  $\text{W m}^{-2}$ , and relative differences are in %.

both due to the filling of missing angles in the ADMs using model results and due to the spatial variability of the anisotropic factor of the Antarctic snow surface is small when averaged over time.

[30] Although the fluxes derived from applying  $ADM_{ed3}$  and  $ADM_{replace}$  to the same radiances agree to within a few  $W m^{-2}$ , this reflects only the fact that the angular distribution of radiance in the CERES ADMs agrees fairly well with the distribution in the model; it does not show anything about the absolute accuracy of the CERES-observed or modeled fluxes or radiances.

## 5. Variation in Angular Distribution Models Due to the Atmosphere

[31] Since the method used to develop the CERES ADMs for regions of permanent snow combines all permanent-snow scenes, regardless of surface elevation or atmospheric water vapor or ozone concentrations, it is important to determine how much uncertainty may be introduced into the CERES flux calculations as a result of spatial and temporal variations in  $R$  at the TOA due to atmospheric variations. This section assesses this variation by running the model described in section 2 with a variety of different atmospheres and examining how the TOA  $R$  changes.

[32] Figure 5 shows a selection of the results. The overall message of Figure 5 is that the expected variations in the atmosphere do not have a very large effect on  $R$  at the TOA, as long as  $\theta_v < 70^\circ$ , which is generally the case for CERES observations.

[33] Figures 5a and 5b show the relative change in TOA  $R$  caused by switching from the Dome C summer atmosphere to the subarctic winter (SAW) atmosphere [McClatchey *et al.*, 1972]. There are three main differences between the two atmospheres that are important to solar radiation: the SAW atmosphere contains nearly six times as much water vapor (4.18 mm of precipitable water compared to 0.72 mm) and about 70% more ozone (486 Dobson Units compared to 284 Dobson Units), and it has 56% more atmospheric mass (surface pressure of 1013 mb compared to 650 mb), which affects molecular scattering and the total amount of carbon dioxide. These two atmospheres are nearly the extremes of the summer atmospheres found over ice sheets. Some parts of Greenland or coastal Antarctica may sometimes have more water vapor than the SAW atmosphere; ozone amounts are rarely greater than that in the SAW atmosphere, but may be less than that in the Dome C atmosphere, especially in spring over Antarctica; surface pressure and total water vapor can be slightly lower than the Dome C atmosphere over the higher parts of Antarctica.

[34] Figures 5a and 5b show that variations in the atmosphere above different permanent-snow surfaces are not likely

to introduce significant uncertainty into the CERES radiance-to-flux conversions. At  $\theta_o = 60^\circ$ , the variations in  $R$  are less than 4% at all viewing angles important to CERES, and at  $\theta_o = 80^\circ$ , they exceed 4% only near the forward reflectance peak, a region where  $R$  is likely to vary for other reasons as well, including surface-roughness and snow-grain-shape variations. These variations in TOA  $R$  are less than or similar to day-to-day variations in the surface  $R$  observations from Dome C, discussed in section 3.4 of Hudson *et al.* [2006].

[35] Figures 5c, 5d, and 5e are intended to dissect the various contributions to Figure 5a. They show the effects of individual atmospheric changes with  $\theta_o = 60^\circ$ . An increase in ozone has a significant effect on  $R$  only at very large  $\theta_v$ , a result that also holds true with  $\theta_o = 80^\circ$  (not shown). Likewise, a sixfold increase in column water vapor amount causes less than 1.5% change in  $R$  at most  $\theta_v$ ; this effect approaches 3% at  $\theta_v = 75^\circ$ ,  $\phi = 0^\circ$ , with  $\theta_o = 80^\circ$  (not shown). Increasing the concentration of all well-mixed gases to bring the surface pressure to that of at sea level (the total amounts of water vapor and ozone were not changed) enhances the amount of molecular scattering, causing changes in  $R$  of up to about 2%; this increases to about 6% at large  $\theta_v$  near the principal plane when  $\theta_o = 80^\circ$ .

[36] All of the changes just discussed lower the TOA albedo by about 2.3%, 3.6%, and 1.3% (relative decrease in albedo, from 0.722) for the ozone, water vapor, and pressure changes with  $\theta_o = 60^\circ$ . The relative decrease in albedo caused by switching to the SAW atmosphere is 7.4%, nearly equal to the sum of the three individual changes. These albedo changes can be captured by the CERES algorithms if they occur without significant alterations to  $R$ . At most viewing angles the variation in  $R$  is much less than the albedo change, except for the run with increased surface pressure. The vast majority of permanent-snow scenes lie above 1000 m, meaning such high surface pressure is rare.

[37] Figure 5f shows the relative difference between  $R$  at the TOA and at the surface, with  $\theta_o = 60^\circ$ . Because light reflected by the surface into large nadir angles must travel through a longer atmospheric path to reach the TOA, it is more likely to be absorbed or scattered on the way. This results in the general pattern seen here that the atmosphere decreases  $R$  at large  $\theta_v$ . The change due to the atmosphere is larger in the forward-scattering direction than in the backward-scattering direction because molecular scattering is much more isotropic than the snow-grain scattering, and therefore reduces the magnitude of the strong forward peak observed at the snow surface and causes the  $R$  at the TOA to be more nearly isotropic than  $R$  at the surface. Figure 5e shows the effect of the reduction in the forward peak because of increased atmospheric scattering.

[38] Figure 5 also illustrates the main uncertainty introduced in our analysis through the use of a plane parallel

**Figure 5.** (a and b) Contours of the relative difference (%) between modeled TOA  $R$  above the SAW atmosphere and that above the Dome C atmosphere (a negative difference indicates a lower value over the SAW atmosphere), for solar zenith angles  $60^\circ$  and  $80^\circ$ . (c–e) The relative difference (%) between modeled TOA  $R$  above a modified Dome C atmosphere and that above the standard Dome C atmosphere (a negative difference indicates a lower value above the modified atmosphere), all with solar zenith angle  $60^\circ$ . The modifications were an increase in total column ozone from 284 to 486 Dobson Units, or an increase in total column water vapor from 0.7 to 4.2 mm of precipitable water, or an increase in surface pressure from 650 to 1013 mb (without changing total column ozone or water vapor amounts). (f) The relative difference (%) between the modeled TOA and surface values of  $R$  with the unmodified Dome C atmosphere and solar zenith angle  $60^\circ$  (a negative value indicates  $R$  is lower at the TOA).

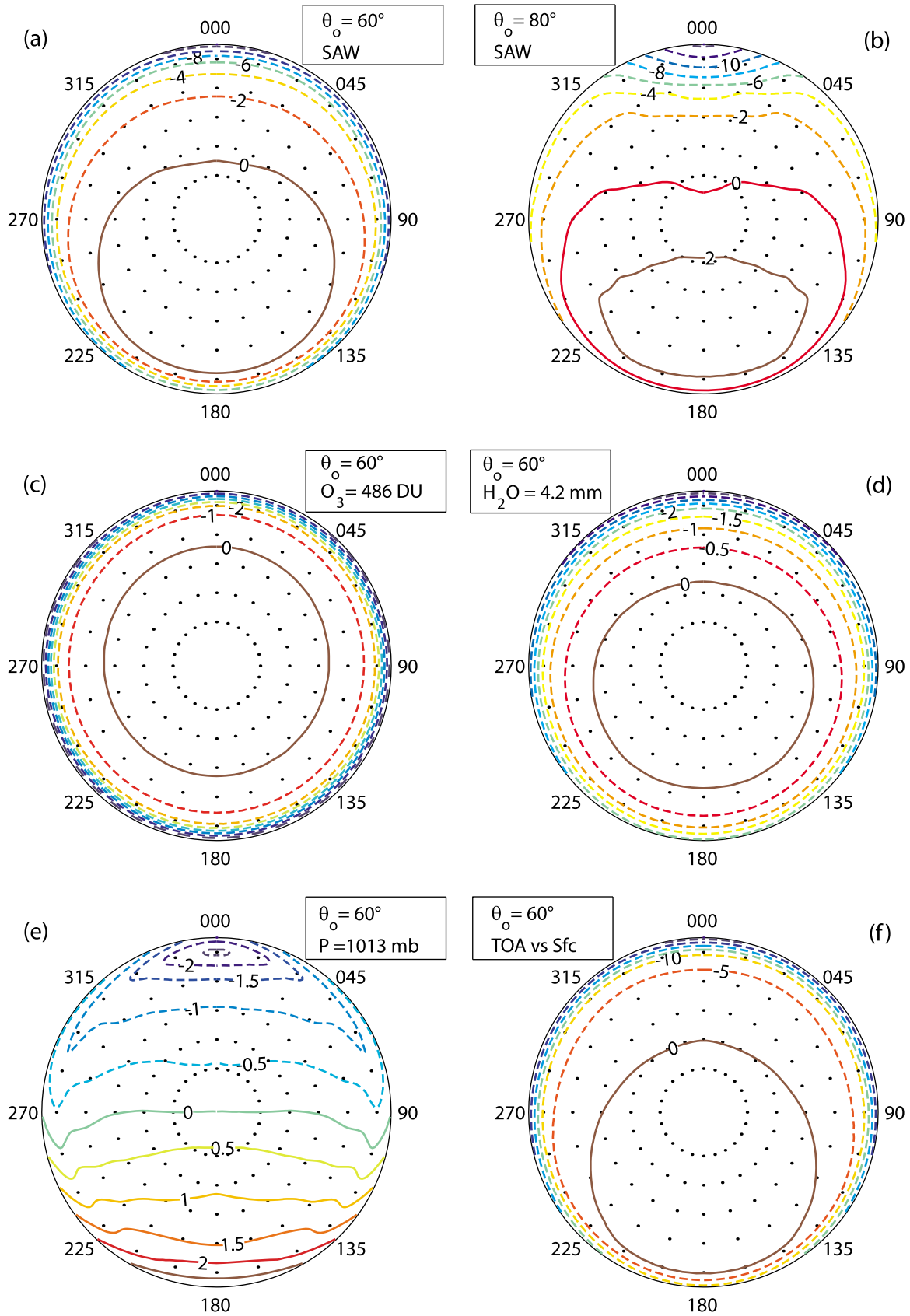


Figure 5

model: too much absorption of light reflected into large viewing zenith angles. Most of the plots in Figure 5 show a sharp decrease in  $R$  at  $\theta_v > 80^\circ$ . Some of this reduction is real due to a longer path length through the atmosphere, but the path length is overestimated by the plane-parallel model, enhancing the reduction. Since the important comparisons with the CERES ADMs are at  $\theta_v < 70^\circ$ , this uncertainty does not cause significant problems in this work.

## 6. Summary

[39] The parameterizations of Hudson *et al.* [2006] provide a realistic lower boundary condition for use in modeling radiative transfer at solar wavelengths over the East Antarctic Plateau. Here they have been extended to cover the full solar spectrum, allowing for the calculation of reflected solar radiance and flux.

[40] The CERES ADMs for permanent-snow scenes were compared with the model results. The angular distribution of the reflected radiance in the ADMs was compared with the model by comparing patterns of  $R$ . These comparisons showed that the CERES permanent-snow ADMs are appropriate for use over Dome C, with their values of  $R$  differing from the modeled values by less than 5% at most geometries.

[41] The uncertainty introduced into the ADMs by filling angles without CERES observations using radiances modeled with a plane-parallel snow surface was examined by recreating the ADMs using the Dome C modeled radiances to fill these angles. Also a new set of ADMs was created using only the Dome C model results. While these changes can cause significant instantaneous changes in flux estimates, the monthly mean, area-averaged changes in flux estimates caused by using the different ADMs are generally less than 2%.

[42] Finally, the effect of the atmosphere and of variations in the atmosphere on TOA  $R$  was examined through modeling results. While the atmosphere significantly alters  $R$  from the values seen at the surface, especially at large  $\theta_v$ , expected variability in atmospheric properties over permanently snow covered areas does not cause large changes to TOA  $R$ . This result shows that the choice to combine all permanently snow covered regions in the development of the ADMs may not limit the accuracy of the CERES fluxes.

[43] **Acknowledgments.** We thank Richard Brandt, Bruce Wielicki, Norman Loeb, Tom Charlock, and Zhonghai Jin for useful discussions and two anonymous reviewers for their helpful comments. This research was supported by National Science Foundation grants OPP-00-03826 and ANT-06-36993. Hudson also received funding from the Norwegian Research Council through its IPY program and the project iAOS Norway (grant number 176096/S30).

## References

Geier, E. B., R. N. Green, D. P. Kratz, P. Minnis, W. F. Miller, S. K. Nolan, and C. B. Franklin (2003), *Clouds and the Earth's Radiant Energy System (CERES) Data Management System Single Satellite Footprint TOA/Surface Fluxes and Clouds (SSF) Collection Document Release 2 Version 1*, NASA Langley Res. Cent., Hampton, Va. (Available at [http://science.larc.nasa.gov/ceres/collect\\_guide/pdf/SSF CG\\_R2V1.pdf](http://science.larc.nasa.gov/ceres/collect_guide/pdf/SSF	CG_R2V1.pdf))

Gettelman, A., V. P. Walden, L. M. Miloshevich, W. L. Roth, and B. Halter (2006), Relative humidity over Antarctica from radiosondes, satellites, and a general circulation model, *J. Geophys. Res.*, *111*, D09S13, doi:10.1029/2005JD006636.

Hudson, S. R., and S. G. Warren (2007), An explanation for the effect of clouds over snow on the top-of-atmosphere bidirectional reflectance, *J. Geophys. Res.*, *112*, D19202, doi:10.1029/2007JD008541.

Hudson, S. R., S. G. Warren, R. E. Brandt, T. C. Grenfell, and D. Six (2006), Spectral bidirectional reflectance of Antarctic snow: Measurements and parameterization, *J. Geophys. Res.*, *111*, D18106, doi:10.1029/2006JD007290.

Jin, Z., and J. J. Simpson (1999), Bidirectional anisotropic reflectance of snow and sea ice in AVHRR channel 1 and 2 spectral regions: Part I. Theoretical analyses, *IEEE Trans. Geosci. Remote Sens.*, *37*, 543–554, doi:10.1109/36.739110.

Kato, S., and N. G. Loeb (2005), Top-of-atmosphere shortwave broadband observed radiance and estimated irradiance over polar regions from Clouds and the Earth's Radiant Energy System (CERES) instruments on Terra, *J. Geophys. Res.*, *110*, D07202, doi:10.1029/2004JD005308.

Leroux, C., and M. Fily (1998), Modeling the effect of sastrugi on snow reflectance, *J. Geophys. Res.*, *103*, 25,779–25,788, doi:10.1029/98JE00558.

Loeb, N. G., K. J. Priestley, D. P. Kratz, E. B. Geier, R. N. Green, B. A. Wielicki, P. O'Rawe Hinton, and S. K. Nolan (2001), Determination of unfiltered radiances from the Clouds and the Earth's Radiant Energy system instrument, *J. Appl. Meteorol.*, *40*, 822–835, doi:10.1175/1520-0450(2001)040<0822:DOURFT>2.0.CO;2.

Loeb, N. G., S. Kato, K. Loukachine, and N. Manalo-Smith (2005), Angular distribution models for top-of-atmosphere radiative flux estimation from the Clouds and the Earth's Radiant Energy System instrument on the Terra satellite: Part I. Methodology, *J. Atmos. Oceanic Technol.*, *22*(4), 338–351, doi:10.1175/JTECH1712.1.

McClatchey, R. A., R. W. Fenn, J. E. A. Selby, F. E. Volz, and J. S. Garing (1972), *Optical Properties of the Atmosphere*, 3rd ed., *Environ. Res. Pap.*, *411*, Air Force Cambridge Res. Lab., Bedford, Mass.

Nakajima, T., and M. Tanaka (1988), Algorithms for radiative intensity calculations in moderately thick atmospheres using a truncation approximation, *J. Quant. Spectrosc. Radiat. Trans.*, *40*(1), 51–69.

Ricchiazzi, P., S. Yang, C. Gautier, and D. Sowle (1998), SBDART: A research and teaching software tool for plane-parallel radiative transfer in the Earth's atmosphere, *Bull. Am. Meteorol. Soc.*, *79*(10), 2101–2114, doi:10.1175/1520-0477(1998)079<2101:SARATS>2.0.CO;2.

Six, D., M. Fily, L. Blarel, and P. Goloub (2005), First aerosol optical thickness measurements at Dome C (East Antarctica), summer season 2003–2004, *Atmos. Environ.*, *32*, 5041–5050, doi:10.1016/j.atmosenv.2005.05.010.

Stamnes, K., S.-C. Tsay, W. Wiscombe, and K. Jayaweera (1988), Numerically stable algorithm for discrete-ordinate-method radiative transfer in multiple scattering and emitting layered media, *Appl. Opt.*, *27*(12), 2502–2509.

Walden, V. P., S. G. Warren, and F. J. Murcray (1998), Measurements of the downward longwave radiation spectrum over the Antarctic Plateau and comparisons with a line-by-line radiative transfer model for clear skies, *J. Geophys. Res.*, *103*, 3825–3846, doi:10.1029/97JD02433.

Warren, S. G., R. E. Brandt, and P. O'Rawe Hinton (1998), Effect of surface roughness on bidirectional reflectance of Antarctic snow, *J. Geophys. Res.*, *103*, 25,789–25,807, doi:10.1029/98JE01898.

Wielicki, B. A., B. R. Barkstrom, E. F. Harrison, R. B. Lee III, G. L. Smith, and J. E. Cooper (1996), Clouds and the Earth's Radiant Energy System (CERES): An Earth Observing System experiment, *Bull. Am. Meteorol. Soc.*, *77*(5), 853–868.

S. R. Hudson, Norwegian Polar Institute, Polar Environmental Centre, N-9296 Tromsø, Norway. (hudson@npolar.no)

S. Kato, Climate Science Branch, NASA Langley Research Center, Mail Stop 420, Hampton, VA 23681-2199, USA. (seiji.kato@nasa.gov)

S. G. Warren, Department of Atmospheric Sciences, University of Washington, Box 351640, Seattle, WA 98195-1640, USA. (sgw@atmos.washington.edu)